DALTON
FULL PAPER

Structure and luminescence of the neutral dinuclear lanthanide(III) complexes [{Ln(api)}$_2$] {H_3api = 2-(2-hydroxyphenyl)-1,3-bis[4-(2-hydroxyphenyl)-3-azabut-3-enyl]-1,3-imidazolidine}

Robertha C. Howell,[a] Kirk V. N. Spence,[a] Ishenkumba A. Kahwa *,†,[a] and David J. Williams[b]

[a] *Chemistry Department, University of the West Indies, Mona, Kingston 7, Jamaica*
[b] *Chemical Crystallography Laboratory, Department of Chemistry, Imperial College of Science, Technology and Medicine, South Kensington, London, UK SW7 2AY*

Dinuclear compounds of lanthanide(III) (Ln^{3+}) ions with api^{3-} [{Ln(api)}$_2$] {H_3api = 2-(2-hydroxyphenyl)-1,3-bis[4-(2-hydroxyphenyl)-3-azabut-3-enyl]-1,3-imidazoline} were synthesized and characterized in microcrystalline form and frozen aqueous solutions in order to establish the ability of triply charged chelates to stabilize Ln^{3+}–Ln^{3+} couples. The crystal structure of the [{Sm(api)}$_2$] complex confirms the dinuclear sandwich binding in which the pair of Ln^{3+} ions is trapped between the two chelates to yield an eight-fold *ca*. square antiprismatic co-ordination geometry on each Ln^{3+} ion. Luminescence decay dynamic studies revealed thermal quenching of $Tb^{3+}(^5D_4)$ [thermal barrier $E_a \approx (1.2 \pm 0.2) \times 10^3$ cm^{-1}] and $Eu^{3+}(^5D_0)$ [$E_a \approx (4.7 \pm 0.2) \times 10^3$ cm^{-1}] emission from [{Tb(api)}$_2$] and [{Eu(api)}$_2$] respectively. Luminescence decay dynamics of homodinuclear [{Ln(api)}$_2$] (Ln = La, Gd, Eu or Tb) and heterodinuclear [{$Tb_{1-x}Eu_x$(api)}$_2$] complexes in polycrystalline and frozen aqueous solutions as well as the small proton NMR relaxivity of [{Gd(api)}$_2$] and low toxicity (to mice) of [{La(api)}$_2$] show qualitatively that members of the [{Ln(api)}$_2$] system are stable in water and merit further study in search of potentially useful tunable biomedical probes.

Several homo- and hetero-dinuclear complexes featuring coupled lanthanide(III) ions (Ln^{3+}) have been prepared and characterized crystallographically[1–3] and spectroscopically.[1,2,4–10] The most successful chromoionophoric templates for lanthanide(III) dinucleation have so far been phenolic Schiff bases (*e.g.* L^1–L^4) but bipyridyl macrocycles such as L^5 have recently shown remarkable potential.[9] Such dinuclear phenolic and bipyridyl lanthanide(III) complexes have demonstrated Ln^{3+}–Ln^{3+} tunable electronic behaviour which is not only of interest in its own right,[4–8] but is also of potential benefit to photonic devices[11] and nuclear magnetic resonance imaging (MRI) techniques which employ paramagnetic ions to enhance image quality.[12] However, factors governing the formation of Ln^{3+}–Ln^{3+} couples and their subsequent entrapment by dinucleating chelates remain largely obscure. With phenolic ligands the importance of a large chelate negative charge-to-lanthanide(III) ion ratio (ρ) to the dinucleation process was indicated by the greater stability of acyclic dinuclear complexes [{$LnL^1(NO_3)$}$_2$], in which ρ = 2 : 1, compared to dinuclear macrocyclic complexes with a lower ρ = 1 : 1 such as [{$LnL^2(NO_3)_2$}$_2$]·$2H_2O$ and [$LnL^3(NO_3)_2$].[8] This dependency of the Ln^{3+} dinucleation process on ρ is reasonable because of the hard Lewis acidity of Ln^{3+} ions. So ρ could indeed be an important molecular design parameter for new types of photonic devices and MRI contrast agents which take advantage of the tunable co-operative electronic behaviour of Ln^{3+}–Ln^{3+} couples. Owing to our interest in the fundamental nature of Ln^{3+}–Ln^{3+} coupling processes and the development of devices based on them, we sought to confirm this hypothesis and employed a triply charged chelate api^{3-} which has a higher ρ = 3 : 1[13] for the purpose. Lanthanide(III) compounds of api^{3-} are very attractive because they are neutral, which is an important consideration in biomedical applications where low osmolarities are desired.[13]

† E-Mail: ikahwa@uwimona.edu.jm

Experimental

Materials

Lanthanide nitrates were prepared by neutralization of respective 99.9% (at least 99.99% for samples used in luminescence studies) sesquioxides Ln_2O_3 (Tb_4O_7 for terbium samples) obtained from Aldrich. Triethylenetetramine and salicylaldehyde were from BDH and of 60 and 99% purity respectively.

Preparation of [{Ln(api)}$_2$]

The non-template reaction of salicylaldehyde with triethylenetetramine followed by $Ln(NO_3)_3$·nH_2O yields compounds of the general stoichiometry [{Ln(api)}$_2$]·nH_2O (n = 0–2).[13] The crystalline anhydrates, [{Ln(api)}$_2$], for this study were prepared by the following template procedure: salicylaldehyde (3 mmol) was dissolved in methanol (200 cm^3) along with $Ln(NO_3)_3$·nH_2O (1 mmol) and then refluxed for 1 h. An excess of triethylenetetramine (4 mmol) was then added and the solution refluxed for 2 d to complete the crystallization process. The crystalline products were harvested (30–40% yield) and dried by rolling them gently on tissue paper. The crystals were of similar morphology and representative elemental analyses were consistent with the unsolvated stoichiometry, [{Ln(api)}$_2$] (Found: C, 53.14; H, 4.53; N, 9.36. $C_{27}H_{27}N_4O_3Sm$ requires C, 53.52; H, 4.49; N, 9.25. Found: C, 52.45; H, 4.37; N, 9.26. $C_{27}H_{27}N_4O_3Tb$ requires C, 52.78; H, 4.43; N, 9.12. Found: C, 51.91; H, 4.30; N, 9.13. $C_{27}H_{27}ErN_4O_3$ requires C, 52.06; H, 4.37; N, 9.00%). The mixed [{$Tb_{1-x}Eu_x$(api)}$_2$] compounds were prepared in a similar fashion after allowing for the desired amounts of terbium(III) and europium(III).

Analyses

Carbon, hydrogen and nitrogen analyses were performed by Medac Ltd., Brunel Science Centre, Surrey, UK. Infrared and UV/VIS spectra were obtained using a Perkin-Elmer 1600 series FT-IR and a UV/VIS/NIR Lambda 19 spectrometer

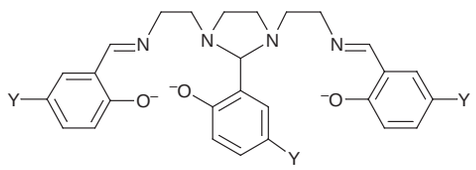

api Y = H
brapi Y = Br

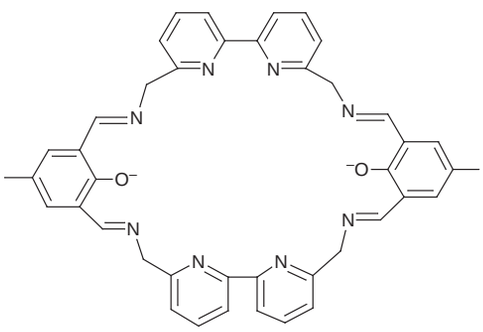

L^5

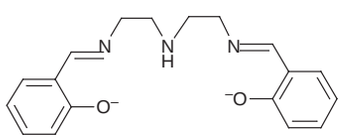

L^1

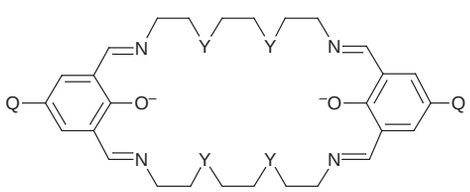

L^2 Y = O, Q = CH_3
L^3 Y = NH, Q = CH_3
L^4 Y = O, Q = Cl

respectively. Proton relaxation rates were measured on a Brüker 200 MHz NMR spectrometer described previously.[14] The Perkin-Elmer LS-5 spectrometer, Photon Technology PL2300 nitrogen and PL201 dye lasers, electronic support and the in-house computational programs used in luminescence studies were described previously.[1,7,15]

Crystallography

Data for [{Sm(api)}$_2$] were collected on a Siemens P4 diffractometer with graphite-monochromated Cu-Kα radiation and ω scans. The data were corrected for Lorentz-polarization and absorption effects (face-indexed numerical correction). The structure was solved by the heavy atom method and non-hydrogen atoms refined anisotropically using F^2 data. All hydrogen atoms were placed in calculated positions and refined isotropically (riding model). All calculations were performed using the SHELXTL program system.[16] A summary of the crystal data and refinement parameters is given in Table 1 and selected bond lengths and angles in Table 2.

CCDC reference number 186/1054.

Results and Discussion

Preparation and structure of [{Ln(api)}$_2$]

Interaction of an excess of triethylenetetramine and salicylaldehyde in the presence of Ln^{3+} ions in methanol yields unsolvated dinuclear complexes of stoichiometry [{Ln(api)}$_2$]. This formulation is consistent with the elemental analyses and infrared spectra which feature the presence of C=N (1638 cm^{-1}) and absence of C=O and N–H absorptions. The most convincing evidence for the preparation of [{Ln(api)}$_2$] is however from a single crystal X-ray diffraction study of [{Sm(api)}$_2$] (Fig. 1). Although the preparation of solvates [{Ln(api)}$_2$]·*n*solv and the crystal structure of a member of a very similar series [{Ln(brapi)}$_2$]·*n*solv, [{La(brapi)}$_2$]·2$CHCl_3$, were reported while our studies were in progress by Orvig's group,[13] it became necessary to determine the structure of the [{Ln(api)}$_2$] compounds because of differences in solvation. Reliable knowledge of the solvent molecules' locations is vital for purposes of interpreting luminescence spectral and decay dynamic studies. Solvation may affect the lanthanide(III) ion site symmetry while O–H[17] and C–H[18] stretching vibrations can quench Ln^{3+} emission. Further, our preliminary luminescence investigations revealed red emission from [{Eu(api)}$_2$] ($^5D_0 \longrightarrow {}^7F_2$) which is forbidden in D_{4d} symmetry that is adopted by the lanthanide(III) co-ordination polyhedron in [{La(brapi)}$_2$]·2$CHCl_3$; the need for firm structural data on the [{Ln(api)}$_2$] series was therefore compelling.

The X-ray analysis shows (Fig. 1) the ligand api^{3-} to have approximate non-crystallographic C_s symmetry about a plane bisecting the central 'imidazolidine' ring and includes the attached phenolate ring which is oriented essentially orthogonally to the imidazolidine ring. The four ligand nitrogen atoms are planar to within 0.01 Å and the two terminal phenolate rings are inclined by *ca*. 25° to this plane. The ligand is heptadentate, and together with a centrosymmetrically related counterpart utilizes all of their potential co-ordinating sites (Fig. 1). The geometry at each Sm^{3+} centre is a slightly distorted square antiprism (Fig. 2) with Sm–O distances in the range 2.273(4)–2.397(3) Å and Sm–N varying between 2.525(4) and 2.831(4) Å, those to the imidazolidine ring nitrogen atoms being significantly longer than those to the imino nitrogens (Table 2). The two co-ordination polyhedra are edge linked about the O(34)···O(34′) vector (2.70 Å) (Fig. 2) with an intramolecular Sm···Sm separation of 3.9176(5) Å. The shortest inter-dimer Sm···Sm distance is 9.60 Å. An inspection of the packing of the dimers reveals only weak π stacking (3.7 Å interplanar separation) between the terminal phenolate rings of adjacent molecules, the overall intermolecular interactions being essentially van der Waals in nature.

By comparison the crystal structure of [{La(brapi)}$_2$]·

Table 1 Summary of crystallographic data

Formula	$C_{54}H_{54}N_8O_6Sm_2$
T/K	293(2)
M	1211.8
Crystal system	Monoclinic
Space group	$P2_1/n$ (no. 14)
a/Å	11.056(1)
b/Å	18.812(1)
c/Å	11.734(2)
β/°	96.81(1)
U/Å^3	2423.3(5)
Z	2
D_c/g cm^{-3}	1.661
μ(Cu-Kα)/mm^{-1}	18.50
Transmission factor range	0.150–0.413
2θ Limit/°	127
No. intensities measured	4196
No. unique intensities	3973
No. intensities with $I > 2\sigma(I)$	3343
No. parameters refined	317
$R1$[a]	0.0363
$wR2$[b]	0.0886

[a] $\Sigma||F_o| - |F_c||/\Sigma|F_o|$. [b] $[\Sigma w(F_o^2 - F_c^2)^2/\Sigma w(F_o^2)^2]^{\frac{1}{2}}$.

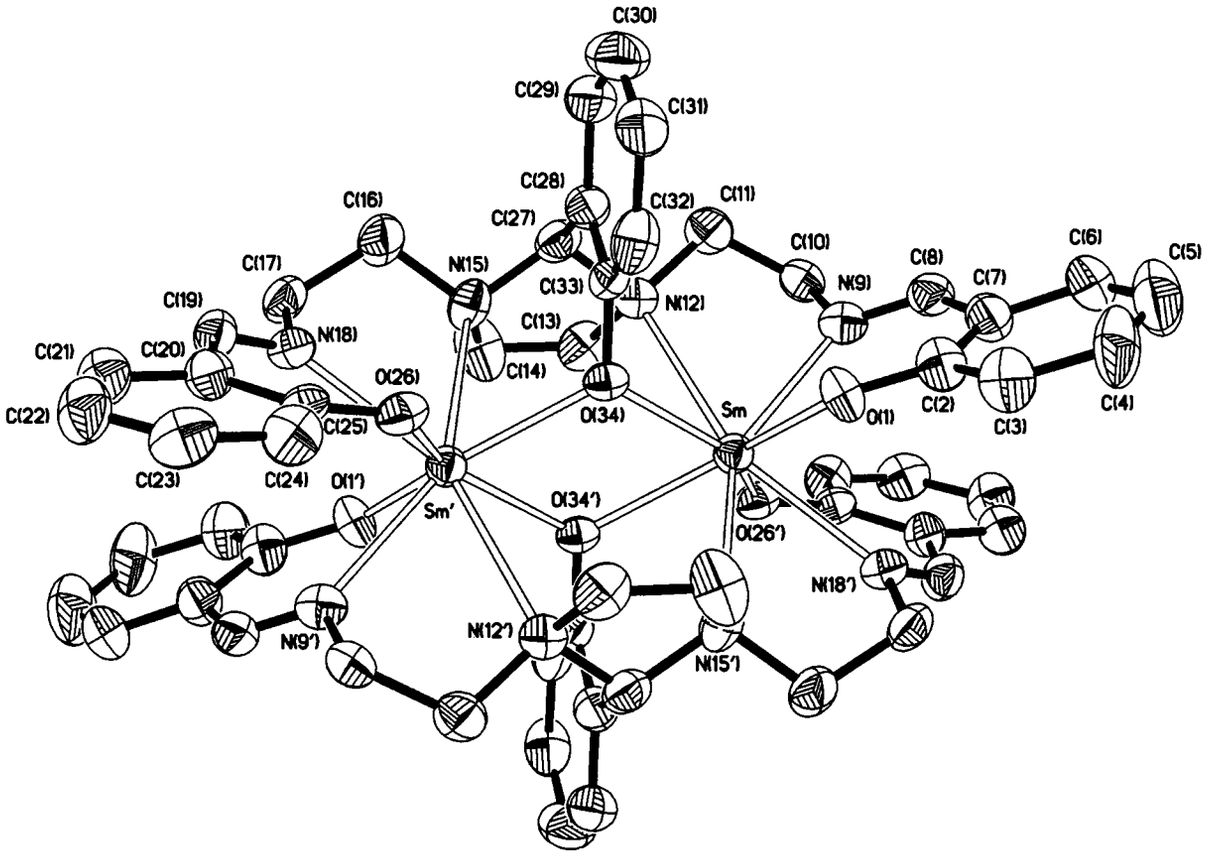

Fig. 1 The dimeric sandwich molecular structure of [{Sm(api)}$_2$] with displacement ellipsoids at 50% probability

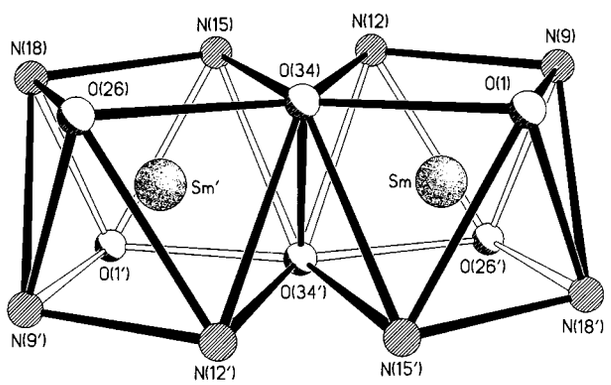

Fig. 2 The approximate square antiprismatic geometry around each Sm^{3+} ion in [{Sm(api)}$_2$]

$2CHCl_3$ features a monoclinic cell with a significantly larger β angle (116.86°) than the one found in [{Sm(api)}$_2$] (96.81°) and a different space group *C*2/*c*. However, both [{La(brapi)}$_2$] and [{Sm(api)}$_2$] dimers are centrosymmetric and their Ln^{3+} ions have square antiprismatic co-ordination geometry with distortions in bond angles and distances (allowing for ionic size differences) of roughly similar magnitudes.

Table 2 Selected bond angles (°) and lengths (Å) for [{Sm(api)}$_2$]

O(1)–Sm–O(34′)	140.76(12)	O(1)–Sm–O(26′)	133.37(12)
O(1)–Sm–O(34)	81.01(12)	O(26′)–Sm–O(34′)	83.17(12)
O(34′)–Sm–O(34)	69.77(12)	O(26′)–Sm–O(34)	143.04(11)
O(26′)–Sm–N(18′)	71.38(14)	O(1)–Sm–N(18′)	74.37(14)
O(34)–Sm–N(18′)	142.64(13)	O(34′)–Sm–N(18′)	114.65(12)
O(26′)–Sm–N(9)	75.75(14)	O(1)–Sm–N(9)	71.60(14)
O(34)–Sm–N(9)	111.74(12)	O(34′)–Sm–N(9)	143.32(12)
O(1)–Sm–N(15′)	81.05(13)	N(18′)–Sm–N(9)	86.73(14)
O(34′)–Sm–N(15′)	70.19(11)	O(26′)–Sm–N(15′)	111.52(14)
N(18′)–Sm–N(15′)	65.87(13)	O(34)–Sm–N(15′)	83.06(12)
O(1)–Sm–N(12)	111.33(13)	N(9)–Sm–N(15′)	145.73(12)
O(34′)–Sm–N(12)	83.21(11)	O(26′)–Sm–N(12)	82.38(13)
N(18′)–Sm–N(12)	145.35(13)	O(34)–Sm–N(12)	70.16(11)
N(15′)–Sm–N(12)	147.53(12)	N(9)–Sm–N(12)	64.67(13)
Sm–O(1)	2.273(4)	Sm–O(34)	2.397(3)
Sm–O(34′)	2.378(3)	Sm–N(9)	2.534(4)
Sm–N(18′)	2.525(4)	Sm–N(12)	2.831(4)
Sm–N(15′)	2.813(4)	Sm–Sm′	3.9176(5)
Sm–O(26′)	2.290(4)		

Luminescence behaviour

The main interest in complexes of [{Ln(api)}$_2$] was to test the hypothesis that highly negatively charged ligands result in more stable dinuclear lanthanide(III) complexes.[8] Solution (especially water)-stable dinuclear lanthanide(III) complexes are essential for evaluating the potential use of this type of compound as luminescent biomedical diagnostics and MRI contrast enhancing agents employing tunable electronic Ln^{3+}–Ln^{3+} coupling. The compounds [{Ln(api)}$_2$] are the first examples of structurally well defined neutral lanthanide(III) dinuclear phenolate complexes showing sufficient water solubility and stability to allow for such an evaluation. The other structurally well defined dinuclear lanthanide(III) systems showing good water solubility and stability are the tetracationic bipyridyl–phenolic series $[Ln_2L^5]^{4+}$.[9] A series of very interesting solution luminescence studies have been reported on water-soluble dinuclear lanthanide(III) complexes of 2,6-bis[*N*,*N*′-bis(carboxymethyl)aminomethyl]-4-benzoylphenol.[10] Unfortunately vital structural information in both solution and solid states is lacking but the data on metal–metal interactions are very encouraging. For these reasons, we have studied the luminescence behaviour of the [{Ln(api)}$_2$] and mixed [{$Ln_{1-x}La_x$(api)}$_2$] compounds in both the solution and solid states in the hope of shedding more light on the interaction between solvent molecules, especially water, with electronically coupled homo Ln^{3+}–Ln^{3+} and hetero Ln^{3+}–Ln'^{3+} pairs.

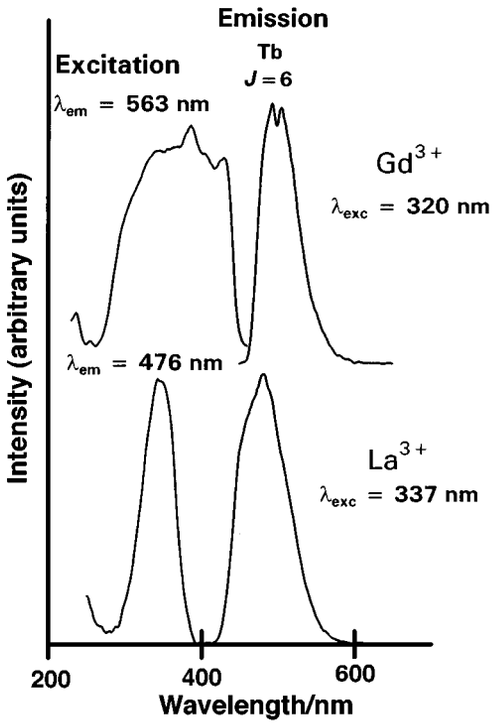

Fig. 3 The 77 K emission (λ_{exc} = 320 and 337 nm) and excitation (λ_{em} = 476 and 563 nm) spectra of [{Ln(api)}$_2$] (Ln = La or Gd). The sharp peak in the emission spectrum of the gadolinium complex is due to sensitized $Tb^{3+}(^5D_4)$ impurities emission

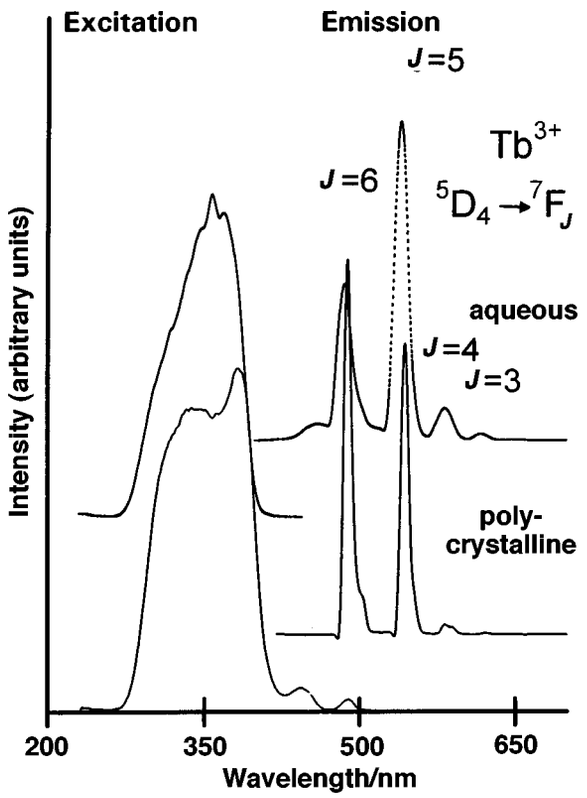

Fig. 4 The 77 K excitation (λ_{em} = 540 nm) and emission (λ_{exc} = 340 nm) spectra of frozen aqueous solution and polycrystalline samples of [{Tb(api)}$_2$]

Photosensitization of Ln^{3+} emission in [{Ln(api)}$_2$] (Ln = Tb or Eu) and [{$Ln_{1-x}La_x$(api)}$_2$]

The electronic absorption spectrum of the [{La(api)}$_2$] complex shows iminophenolate absorptions at 270, 330, 370 and 450 nm which coincide with the broad and complex unresolved absorption envelops of the excitation spectra of ligand emission from both [{La(api)}$_2$] and [{Gd(api)}$_2$] (Fig. 3). Excitation of [{La(api)}$_2$] at 337 nm and 77 K results in complex broad emission (430–600 nm; $\lambda_{max} \approx 480$ nm) while the [{Gd(api)}$_2$] complex yields (also complex) broad emission at longer wavelengths (450–625 nm; $\lambda_{max} \approx 510$ nm) (Fig. 3). The broad emission is presumably from the electronic states of ligands or related organic traps while sharp $Tb^{3+}(^5D_4 \longrightarrow {}^7F_6)$ emission due to sensitization of a Tb^{3+} impurity[8] is seen on the emission spectrum of the [{Gd(api)}$_2$] complex. The good spectral overlap between the intense ligand or trap emission and the $Tb^{3+}(^5D_4)$ state provides suitable conditions for sensitized $Tb^{3+}(^5D_4 \longrightarrow {}^7F_6)$ emission.[19] However, the complexity of the ligand emission spectra and interference from Tb^{3+} impurities preclude detailed assignments.

The [{Tb(api)}$_2$] excitation in the near UV yields typically $Tb^{3+}(^5D_4 \longrightarrow {}^7F_J)$ emission which is very strong at 77 K but weaker at room temperature. The dominant feature in the corresponding 77 K excitation spectrum (λ_{em} = 540 nm) (Fig. 4) is a complex broad absorption at *ca.* 270–420 nm similar to that of [{Ln(api)}$_2$] (Ln = La or Gd) compounds. A weak direct $Tb^{3+}(^5D_4 \longleftarrow {}^7F_6)$ absorption at about 488 nm is also observed. Excitation of [{Eu(api)}$_2$] at 77 K in the near UV produces typical $Eu^{3+}(^5D_0 \longrightarrow {}^7F_J)$ emission the excitation spectrum (λ_{em} = 610 nm) (Fig. 5) of which also shows a poorly resolved broad ligand absorption envelop in the range 280–470 nm and direct $Eu^{3+}(^5D_J \longleftarrow {}^7F_0)$ contributions at 465 (J = 2) and 530 nm (J = 1). A broad emission band in the 400–550 nm region (λ_{max} = 485 nm) (Fig. 5) is also observed. Excitation of the europium(III) complex at 400 nm results in predominantly $Eu^{3+}(^5D_0)$ emission without the anomalous broad peak at 485 nm (Fig. 5) which shows that this peak has origin in the ligand states. Regardless of the excitation wavelength, emission from

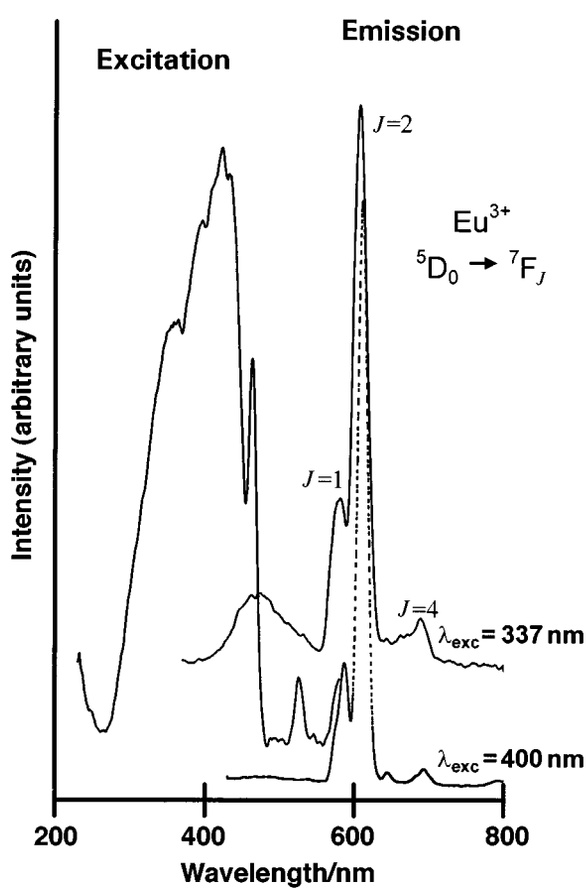

Fig. 5 The 77 K excitation (λ_{em} = 610 nm) and emission (λ_{exc} = 337 or 400 nm) of polycrystalline [{Eu(api)}$_2$]

$Eu^{3+}(^5D_0)$ in [{Eu(api)}$_2$] is dominated by the hypersensitive $^5D_0 \longrightarrow {}^7F_2$ transition which is forbidden as an electric dipole for Eu^{3+} in co-ordination polyhedra of strict D_{4d} symmetry.[20,21]

Table 3 Decay rates (k_i) for $Tb^{3+}(^5D_4)$ and $Eu^{3+}(^5D_0)$ in $[\{Ln(api)\}_2]$

Compound		Excited state[a]	T/K	k_1/s^{-1}	k_2/s^{-1}
$[\{Tb(api)\}_2]$	Polycrystalline	$Tb^{3+}(^5D_4)$	147	2×10^4	1×10^3
	D_2O solution	$Tb^{3+}(^5D_4)$	147	2×10^4	2×10^3
	Aqueous solution	$Tb^{3+}(^5D_4)$	147	2×10^4	2×10^3
$[\{Eu(api)\}_2]$	Polycrystalline	$Eu^{3+}(^5D_0)$	147	3×10^5	2×10^3
	D_2O solution	$Eu^{3+}(^5D_0)$	147	7×10^5	2×10^3
	Aqueous solution	$Eu^{3+}(^5D_0)$	147	9×10^5	3×10^3
$[\{Tb(api)\}_2]$	Polycrystalline	$Tb^{3+}(^5D_4)$	298[b]	1.6×10^5	
$[\{Tb(api)\}_2]$	Polycrystalline	$Tb^{3+}(^5D_4)$	77	1.3×10^3	
$[\{Tb_{1-x}La_x(api)\}_2]$	Polycrystalline	$Tb^{3+}(^5D_4)$	77	1.0×10^3	
$[\{Eu(api)\}_2]$	Polycrystalline	$Eu^{3+}(^5D_0)$	298[b]	8.1×10^4	
$[\{Eu(api)\}_2]$	Polycrystalline	$Eu^{3+}(^5D_0)$	77	2.9×10^3	
$[\{Eu_{1-x}La_x(api)\}_2]$	Polycrystalline	$Eu^{3+}(^5D_0)$	77	1.9×10^3	
$[\{Tb_{1-x}Eu_x(api)\}_2]$	Polycrystalline	$Tb^{3+}(^5D_4)$	77[c]	1×10^5	2×10^3
$[\{Tb_{1-x}Eu_x(api)\}_2]$	Polycrystalline	$Eu^{3+}(^5D_0)$	77[c]	-2×10^5[d]	2×10^3
$[\{Tb_{1-x}Eu_x(api)\}_2]$	D_2O solution	$Tb^{3+}(^5D_4)$	77[c]	1×10^5	2×10^3
$[\{Tb_{1-x}Eu_x(api)\}_2]$	D_2O solution	$Eu^{3+}(^5D_0)$	77[c]	-2×10^5[d]	2×10^3

[a] Direct excitation of terbium was at 488 nm while that of europium was at 577 nm. The $Tb^{3+}(^5D_4)$ and $Eu^{3+}(^5D_0)$ emissions were monitored at 540 and 610 nm respectively. [b] Room temperature emission is weak; estimate of major component is quoted. [c] Samples were excited *via* the ligand state at 337 nm. [d] Negative sign means excitation build-up rate.

However, certain other factors cannot be ignored. The most important ones may be the aromatic electronic clouds (with which the Eu^{3+} is in some contact *via* through-space interactions and the partial double character of the phenolate C–O bonds[22]) and polarization effects[23] due to strong bonding of europium(III) to the four phenolate centres. These considerations may result in the effective crystal electric field symmetry at the Eu^{3+} centre being lower than the *ca.* D_{4d} adopted by the co-ordination polyhedra or trigger the hypersensitive behaviour of the $^5D_0 \longrightarrow {}^7F_2$ transition. Sensitization of both Tb^{3+}-($^5D_4 \longrightarrow {}^7F_J$) (Figs. 3 and 4) and $Eu^{3+}(^5D_0 \longrightarrow {}^7F_2)$ (Fig. 5) emission by the ligand states is evident from the excitation spectra which feature absorptions of the organic chromophore; but emission from organic traps and their involvement in metal emission quenching are good possibilities.

Luminescence decay dynamics

Owing to possible spectral interference of the broad organic-type emission (Figs. 4 and 5) with the metal ion emission, lanthanide(III) luminescence decay data were acquired after exciting directly the $Tb^{3+}(^5D_4)$ and $Eu^{3+}(^5D_0)$ levels at 488 and 577 nm respectively. Luminescence decay rates of $Tb^{3+}(^5D_4)$ and $Eu^{3+}(^5D_0)$ states in pure $[\{Tb(api)\}_2]$ and $[\{Eu(api)\}_2]$ compounds and inert matrices afforded by $[\{Tb_{1-x}La_x(api)\}_2]$ and $[\{Eu_{1-x}La_x(api)\}_2]$ ($x > 0.95$) are shown in Table 3. Single-exponential luminescence decay prevails for $Tb^{3+}(^5D_4)$ and $Eu^{3+}(^5D_0)$ in $[\{Tb_{1-x}La_x(api)\}_2]$ and $[\{Eu_{1-x}La_x(api)\}_2]$ respectively at 77 K but emission is too weak to measure at 298 K. However, the temperature dependence of the decay process is evident, for both $[\{Tb(api)\}_2]$ and $[\{Eu(api)\}_2]$ compounds, from a comparison of the decay rates at 77, 147 and 298 K (Table 3). We therefore studied in detail the temperature evolution of the emission decay rates of $[\{Tb(api)\}_2]$ and $[\{Eu(api)\}_2]$ in order to gain more insight into the nature of the temperature-dependent quenching processes.

The luminescence decay behaviour of $[\{Tb(api)\}_2]$ and $[\{Eu(api)\}_2]$ following direct excitation of the $Tb^{3+}(^5D_4)$ (λ_{exc} = 488 nm) and $Eu^{3+}(^5D_0)$ (λ_{exc} = 577 nm) states is single-exponential and temperature independent in the range 77–140 K for Tb^{3+} and 77–233 K for Eu^{3+}. The corresponding spontaneous decay rates (k_i) are *ca.* 1.1×10^3 and 2.1×10^3 s^{-1} for $Tb^{3+}(^5D_4)$ and $Eu^{3+}(^5D_0)$ respectively. These values are slightly larger than those found for $Tb^{3+}(^5D_4)$ and $Eu^{3+}(^5D_0)$ in inert matrices ($[\{Ln_{1-x}La_x(api)\}_2]$, Ln = Tb or Eu) (Table 3) possibly because of weak concentration quenching associated with energy migration on the lanthanide(III) sublattice. With $T > 140$ K for $[\{Tb(api)\}_2]$ and >230 K for $[\{Eu(api)\}_2]$ temperature-dependent multiexponential decay curves are obtained. In these cases excitation trapping information can be extracted from the observed rates of the fast decaying component (k_f) which, for comparative purposes, can be estimated from fits by double-exponential models. The temperature-dependent k_f data were subsequently used to estimate the trapping rates (k_t) ($k_t = k_f - k_i$); the k_t values so obtained were plotted as $\ln k_t$ *vs.* $1/T$. The corresponding thermal barriers, E_a, for quenching emission from $Eu^{3+}(^5D_0)$ in $[\{Eu(api)\}_2]$ and $Tb^{3+}(^5D_4)$ in $[\{Tb(api)\}_2]$ were found from the slopes of these Arrhenius plots [*i.e.* $\ln k_t = \ln A + (E_a/RT)$ where A and R are the pre-exponential factor and gas constants], to be *ca.* $(4.7 \pm 0.2) \times 10^3$ and $(2.1 \pm 0.2) \times 10^3$ cm^{-1} respectively. We attribute the quenching activity to an organic state (ligand or organic trap impurity) in the vicinity of the *ca.* 22 000 cm^{-1} region. The trapping thermal barriers would, in this case, correspond to the energy required to bridge the $Eu^{3+}(^5D_0)$ (17 200 cm^{-1}) and $Tb^{3+}(^5D_4)$ (20 500 cm^{-1}) energy levels with the organic trapping state. This conclusion is reasonable in view of the weak broad absorptions seen at roughly 440–485 nm (Figs. 4 and 5).

Solution luminescence of $[\{Ln(api)\}_2]$ (Ln = Tb or Eu)

For compounds of potential biomedical diagnostic interest, aqueous solution studies are essential for establishing solubility, stability and toxicity. It was therefore of great interest to study the luminescence behaviour of the $[\{Ln(api)\}_2]$ series in aqueous solutions for comparison with that of the polycrystalline forms, especially at 77 K where quenching activity is minimal (see above). Direct excitation of the $Tb^{3+}(^5D_4)$ and $Eu^{3+}(^5D_0)$ states at 488 and 577 nm respectively produced very weak emission from frozen aqueous solutions of $[\{Eu(api)\}_2]$ and $[\{Tb(api)\}_2]$. Therefore indirect excitation of the frozen aqueous and D_2O solutions *via* ligand absorptions at 337 nm was used to obtain spectra and decay curves for comparison with those of polycrystalline samples. Spectra of frozen D_2O solutions of the $[\{Eu(api)\}_2]$ complex were still too weak to measure. The emission and excitation spectra of $[\{Tb(api)\}_2]$ however were informative (Fig. 4). The excitation spectra of frozen D_2O solutions of $[\{Tb(api)\}_2]$ are similar to those of the polycrystalline compound, but the emission spectra show subtle differences especially in the intensity (area) ratio of the $^5D_4 \longrightarrow {}^7F_6$: $^5D_4 \longrightarrow {}^7F_5$ peaks. This ratio changes from 1.3:1 in polycrystalline $[\{Tb(api)\}_2]$ to the more normal 0.6:1 for the corresponding frozen D_2O solution (Fig. 4). Intensity changes usually reflect modifications in the crystal electric field symmetry around the Tb^{3+} ion, which affect selection rules. Since there are no noticeable changes in the excitation spectrum dominated by

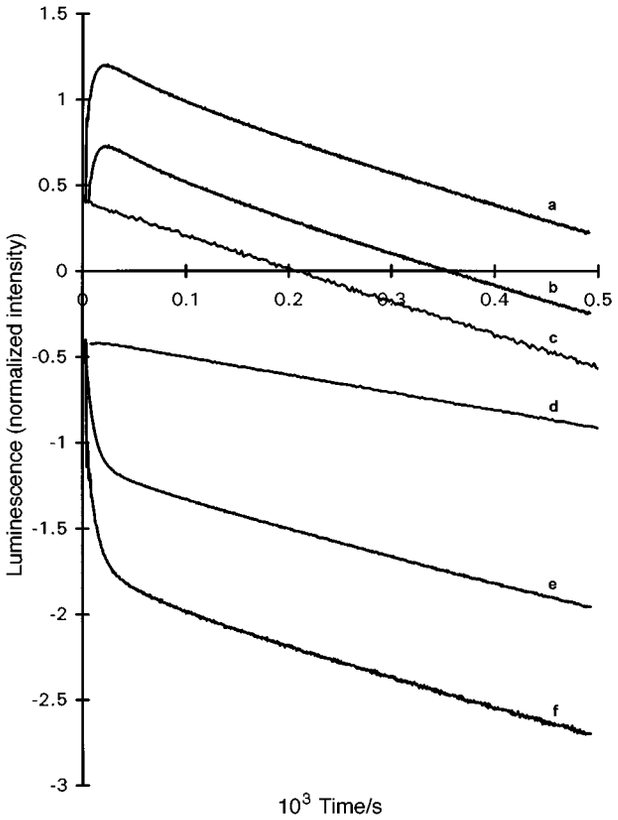

Fig. 6 The 77 K decay curves for $Eu^{3+}(^5D_0)$ ($\lambda_{em} = 610$ nm) and $Tb^{3+}(^5D_4)$ ($\lambda_{em} = 540$ nm) in $[\{Tb_{1-x}Eu_x(api)\}_2]$ {frozen aqueous solutions [a, $Eu^{3+}(^5D_0)$; f, $Tb^{3+}(^5D_4)$]; polycrystalline solid [b, $Eu^{3+}(^5D_0)$; e, $Tb^{3+}(^5D_4)$]} compared to the decay curve profiles of the pure homodinuclear polycrystalline samples, $[\{Eu(api)\}_2]$ [c, $Eu^{3+}(^5D_0)$] and $[\{Tb(api)\}_2]$ [d, $Tb^{3+}(^5D_4)$]. The samples were excited at 337 nm

ligand absorption, it is reasonable to conclude that dissolution of the $[\{Tb(api)\}_2]$ compound in water did not change the terbium(III)–api interaction significantly. Analysis of the long-time decay data (k_2) in frozen D_2O and aqueous solutions of both $[\{Tb(api)\}_2]$ and $[\{Eu(api)\}_2]$ (Table 3) using the Horrocks–Sudnick relation[17] $q = A(k_{H_2O} - k_{D_2O})$, where $A = 4.2 \times 10^{-3}$ for $Tb^{3+}(^5D_4)$ and 1.05×10^{-3} for $Eu^{3+}(^5D_0)$, indicates that the Ln^{3+} centres interact, on average, with roughly one co-ordinated water molecule. It seems that either the co-ordination number of the Ln^{3+} ion changes in aqueous solution to nine to accommodate a water molecule or the complex dissociates into monohydrated monomers $[Ln(api)(H_2O)]$. To check these possibilities we studied the luminescence behaviour of the heterodinuclear complex $[\{Tb_{1-x}Eu_x(api)\}_2]$ in the hope that the luminescence decay behaviour of the Tb^{3+}–Eu^{3+} couple in heterodinuclear $[TbEu(api)_2]$ molecules would shed more light on the integrity of $[\{Ln(api)\}_2]$ molecules in water.

The 77 K luminescence decay curves of $Tb^{3+}(^5D_4)$ and $Eu^{3+}(^5D_0)$ in polycrystalline $[\{Tb_{1-x}Eu_x(api)\}_2]$ and its frozen D_2O solutions are compared in Fig. 6. The two sets of $Eu^{3+}(^5D_0)$ decay curves (Fig. 6a and 6b) are similar and exhibit excitation build-ups (*ca.* 2×10^5 s^{-1}) not seen with $Eu^{3+}(^5D_0)$ in pure $[\{Eu(api)\}_2]$ or the inert matrix of $[\{La_{1-x}Eu_x(api)\}_2]$ (Fig. 6c). This excitation build up corresponds to the quick decay component (*ca.* 1×10^5 s^{-1}) of $Tb^{3+}(^5D_4)$ emission for both polycrystalline (Fig. 6e) and frozen D_2O solutions of $[\{Tb_{1-x}Eu_x(api)\}_2]$ (Fig. 6f) which, also, is not found on decay curves of $[\{Tb(api)\}_2]$ or $[\{La_{1-x}Tb_x(api)\}_2]$ (Fig. 6d). The slow decaying component of $Tb^{3+}(^5D_4)$ emission (77 K) from polycrystalline or frozen solutions of $[\{Tb_{1-x}La_x(api)\}_2]$ (*ca.* 2×10^3 s^{-1}) is of the same order of magnitude as that of $[\{Tb(api)\}_2]$ or $[\{Tb_{1-x}La_x(api)\}_2]$ (Table 3); we attribute this slow component to the homodinuclear $[\{Tb(api)\}_2]$ molecules.

We thus assign an intramolecular $Tb^{3+}(^5D_4)$-to-Eu^{3+} energy transfer rate of *ca.* 10^5 s^{-1} and conclude that the Tb^{3+}–Eu^{3+} coupling of heterodinuclear dimers $[TbEu(api)_2]$ remains largely intact in aqueous solutions. Assuming that the intramolecular Tb^{3+}–Eu^{3+} interaction responsible for Tb^{3+}-to-Eu^{3+} energy transfer across the phenolate bridge is predominantly dipolar in nature, the corresponding coupling constant, c, is weak and estimated to be *ca.* 4×10^{-52} m^6 s^{-1} from the Förster–Dexter equation ($k = c/r^6$).[24,25] We thus conclude that the $[\{Ln(api)\}_2]$ compounds, especially those of the heavy lanthanide(III), are more stable in solution than previously known dinuclear complexes of L^1–L^4 and that indeed highly charged ligands are important for the stabilization of coupled lanthanide(III) ions. The subtle spectral changes upon dissolving $[\{Tb(api)\}_2]$ in water (Fig. 4) are thus largely due to the introduction of water molecules into the co-ordination sphere without destroying dinuclearity, *i.e.* $[\{Ln(api)(H_2O)\}_2]$. However, a small degree of dissociation cannot be ruled out without the benefit of high-resolution spectral studies.

Proton NMR relaxivity studies

The solution stability of $[\{Ln(api)(H_2O)\}_2]$ (aq) indicated by the above luminescence decay dynamic results encouraged us to study the water ^1H relaxation characteristics of aqueous $[\{Gd(api)\}_2]$ in search of features of interest to contrast enhancement in MRI. Preliminary results show that the water ^1H relaxivity at 25 °C, approximately 5.7×10^{-2} mM^{-1} s^{-1}, is low. This is consistent with the conclusion that the $[\{Ln(api)\}_2]$ complexes are not dissociated in aqueous solutions and exchange between co-ordinated and solution water molecules is very restricted, presumably because the metal ions are well sheltered from the solution environment by the organic moieties (Fig. 1). These results were collaborated by toxicological studies[26] which revealed that, compared to dinuclear complexes of L^1–L^4 which were fatal to rats at low doses, $[\{La(api)\}_2]$ features very low toxicity even when the doses were increased fivefold.

Conclusion

The preponderance of structural, luminescence, NMR and toxicity evidence on $[\{Ln(api)\}_2]$ presented here shows qualitatively that these compounds are more stable than previously known dinuclear complexes of L^1–L^4 and that indeed ρ is an important molecular design parameter in the development of compounds featuring Ln^{3+}–Ln^{3+} couples. Whereas information on the aqueous stability constants and factors promoting better proton NMR relaxivities of $[\{Ln(api)\}_2]$ is still required for a detailed evaluation of their potential, their low toxicities and the good stability of complexes of L^5 should encourage further investigations of the phenolate lanthanide(III) dinuclear complexes in search of potential biomedically useful systems.

Acknowledgements

We thank the Leverhulme Trust for supporting work at the University of the West Indies (UWI) (Grant no. F/709A) and the British Council/UWI CICHE programme for supporting the Imperial College–UWI collaboration. The write-up was done with financial assistance from the InterAmerican Development Bank–UWI Development programme (R&D Project no. 29).

References

1 K. D. Matthews, I. A. Kahwa and D. J. Williams, *Inorg. Chem.*, 1994, **33**, 1382.
2 I. A. Kahwa, S. Folkes, D. J. Williams, S. V. Ley, C. A. O'Mahoney and G. L. McPherson, *J. Chem. Soc., Chem. Commun.*, 1989, 1531.

3 J. M. Harrowfield, M. I. Ogden, A. H. White and F. R. Wilner, *Aust. J. Chem.*, 1989, **42**, 949; J. M. Harrowfield, M. I. Ogden and A. H. White, *Aust. J. Chem.*, 1991, **44**, 1237, 1249; B. M. Furphy, J. M. Harrowfield, D. L. Kepert, B. W. Skelton, A. H. White and F. R. Wilner, *Inorg. Chem.*, 1987, **26**, 4231.
4 I. A. Kahwa, J. Selbin, T.-C. Y. Hsieh and R. A. Laine, *Inorg. Chim. Acta*, 1986, **118**, 179.
5 P. Guerriero, P. A. Vigato, J.-C. G. Bünzli and E. Moret, *J. Chem. Soc.*, *Dalton Trans.*, 1990, 647.
6 K. D. Matthews, S. A. Bailey-Folkes, I. A. Kahwa, C. A. O'Mahoney, S. V. Ley, D. J. Williams, C. J. Groombridge and C. J. O'Connor, *J. Phys. Chem.*, 1992, **96**, 7021.
7 K. D. Matthews, R. A. Fairman, A. Johnson, K. V. N. Spence, I. A. Kahwa, G. L. McPherson and H. Robotham, *J. Chem. Soc.*, *Dalton Trans.*, 1993, 1719.
8 R. C. Howell, K. V. N. Spence, I. A. Kahwa, A. J. P. White and D. J. Williams, *J. Chem. Soc.*, *Dalton Trans.*, 1996, 961.
9 Z. Wang, J. Reibenspies and A. E. Martell, *Inorg. Chem.*, 1997, **36**, 629.
10 M. Latva, P. Mäkinen, S. Kulmala and K. Haapakka, *J. Chem. Soc.*, *Faraday Trans.*, 1996, **92**, 3321; M. Latva, S. Kulmala and K. Haapakka, *Inorg. Chim. Acta*, 1996, **247**, 209.
11 N. Sabbatini, M. Guardigli and J.-M. Lehn, *Coord. Chem. Rev.*, 1993, **123**, 201.
12 S. Aime, M. Botta, M. Fasano and E. Terreno, *Chem. Soc. Rev.*, 1998, 19.
13 L.-W. Yang, S. Liu, E. Wong, S. J. Rettig and C. Orvig, *Inorg. Chem.*, 1995, **34**, 2164.
14 D. M. Y. Barrett, I. A. Kahwa, J. T. Mague and G. L. McPherson, *J. Org. Chem.*, 1995, **60**, 5946.
15 R. A. Fairman, K. V. N. Spence and I. A. Kahwa, *Rev. Sci. Instrum.*, 1995, **65**, 503.
16 G. M. Sheldrick, SHELXTL, version 5.03, Siemens Analytical X-Ray Instruments, Madison, WI, 1994.
17 W. DeW. Horrocks and D. R. Sudnick, *Acc. Chem. Res.*, 1981, **14**, 384.
18 R. S. Dickens, D. Parker, A. S. deSousa and J. A. G. Williams, *Chem. Commun.*, 1996, 697.
19 R. D. Archa, H. Chen and L. C. Thompson, *Inorg. Chem.*, 1998, **37**, 2089; M. Latva, H. Takalo, V.-M. Mukkala and J. Kankare, *Inorg. Chim. Acta*, 1998, **267**, 63.
20 G. Blasse, *Inorg. Chim. Acta*, 1988, **142**, 153.
21 L. C. Thompson and S. C. Kuo, *Inorg. Chim. Acta*, 1988, **149**, 305.
22 I. A. Kahwa, F. R. Fronczek and J. Selbin, *Inorg. Chim. Acta*, 1987, **126**, 232.
23 B. Stewart, in *Mathematical and Physical Sciences*, NATO ASI Series C, ed. C. D. Flint, Kluwer, Dordrecht, 1989, vol. 288, p. 327.
24 D. L. Dexter, *J. Chem. Phys.*, 1953, **21**, 836.
25 Th. Förster, *Ann. Phys.* (*Leipzig*), 1948, **2**, 55.
26 L. A. D. Williams, R. Howell, I. A. Kahwa and R. E. Young, unpublished work.

Received 1*st June* 1998; *Paper* 8/04056G